Analyst

PAPER

View Article Online
View Journal | View Issue

Cite this: *Analyst*, 2014, **139**, 3991

A highly sensitive NADH sensor based on a mycelium-like nanocomposite using graphene oxide and multi-walled carbon nanotubes to co-immobilize poly(luminol) and poly(neutral red) hybrid films†

Kuo Chiang Lin, Szu Yu Lai and Shen Ming Chen*

Received 24th March 2014
Accepted 8th May 2014

DOI: 10.1039/c4an00536h

www.rsc.org/analyst

Hybridization of poly(luminol) (PLM) and poly(neutral red) (PNR) has been successfully performed and further enhanced by a conductive and steric hybrid nanotemplate using graphene oxide (GO) and multi-walled carbon nanotubes (MWCNTs). The morphology of the PLM–PNR–MWCNT–GO mycelium-like nanocomposite is studied by SEM and AFM and it is found to be electroactive, pH-dependent, and stable in the electrochemical system. It shows electrocatalytic activity towards NADH with a high current response and low overpotential. Using amperometry, it has been shown to have a high sensitivity of 288.9 μA mM^{-1} cm^{-2} to NADH ($E_{app.}$ = +0.1 V). Linearity is estimated in a concentration range of 1.33 × 10^{-8} to 1.95 × 10^{-4} M with a detection limit of 1.33 × 10^{-8} M (S/N = 3). Particularly, it also shows another linear range of 2.08 × 10^{-4} to 5.81 × 10^{-4} M with a sensitivity of 151.3 μA mM^{-1} cm^{-2}. The hybridization and activity of PLM and PNR can be effectively enhanced by MWCNTs and GO, resulting in an active hybrid nanocomposite for determination of NADH.

1. Introduction

Reduced β-nicotinamide adenine dinucleotide (NADH) and its oxidized form, NAD^+, are very important coenzymes that play an important role in the energy production/consumption of cells of all living organisms. NADH participates in a variety of enzymatic reactions *via* more than 300 dehydrogenases.[1] Many studies have focused on the fundamental scientific applications of the NADH reaction. Numerous analytical methods have been proposed for NADH detection, including colorimetry,[2] fluorescence,[3] enzymatic assay,[4] high-performance liquid chromatography,[5] electrospray ionization mass spectrometry,[6] capillary electrophoresis,[7] and electrochemical assays.[8,9] It has received considerable interest due to its very important role as a cofactor in a whole diversity of dehydrogenase-based bioelectrochemical devices such as biosensors, biofuel cells, and bioreactors.[10–12] However, direct oxidation of NADH at a conventional solid electrode is highly irreversible, requires large activation energy, and proceeds with coupled side reactions, poisoning the electrode surface.[13–15] In recent years, many nanomaterials, especially various carbon nanomaterials,[16–18] have been widely used to reduce the overpotential for NADH oxidation and minimize the surface contamination effect without the help of redox mediators.

Over the last two decades, carbon nanotubes (CNTs) have gained increasing popularity due to their unique properties such as electronic, metallic and structural characteristics.[19] CNTs have outstanding ability to mediate fast electron transfer kinetics for a wide range of electroactive species and show electrocatalytic activity towards biologically important compounds such as NADH and H_2O_2.[20,21] Recently, the fabrication of CNT/conducting polymer composites has gained great interest as the CNTs can improve the electrical and mechanical properties of polymers[22,23] and it has been demonstrated that the obtained CNT/conducting polymer composites possess properties of the individual components with a synergistic effect.[24–29] Particularly, CNTs might play a role as a template in the immobilization of conducting polymers especially for the hybridization of different conducting polymers.

Graphene oxide (GO) consists of a single atomic layer of sp^2-hybridized carbon atoms functionalized mainly with phenol, hydroxyl, and epoxide groups on the basal plane and ionizable carboxyl groups at the edges; it is obtained after treating graphite with strong oxidizers. GO can form stable single-layer aqueous dispersions due to the charge repulsion of the ionized edge acid groups. As a derivatized graphite nanomaterial, GO features a highly hydrophobic surface with non-oxidized

Electroanalysis and Bioelectrochemistry Lab, Department of Chemical Engineering and Biotechnology, National Taipei University of Technology, no.1, Section 3, Chung-Hsiao East Road, Taipei 106, Taiwan. E-mail: smchen78@ms15.hinet.net; Fax: +886-2-27025238; Tel: +886-2-27017147

† Electronic supplementary information (ESI) available. See DOI: 10.1039/c4an00536h

polyaromatic nanographene domains on the basal plane. The abundance of highly conjugated structures on the surface of GO allows it to adhere readily to conjugated materials through π–π interactions, making GO function as a unique tethered 2D surfactant sheet.[30–35]

Recently, many studies have confirmed that GO is a good candidate for use as an advanced carbon material in electrochemical applications.[36–38] Because CNTs and GO exhibit many similar properties, while being structurally dissimilar, covalent preparation of rGO/CNT composites provides attractive building blocks for the development of nanocarbon materials with potentially improved conductivity and catalytic ability for electrochemical research.

Luminol (LM) has been widely used in chemiluminescence detection,[39] electrochemiluminescence,[40,41] as well as for immunoassays using a flow injection system and liquid chromatography.[42,43] A polyluminol (PLM) film modified on the working electrode provides a reversible redox couple involving electron transfer. As demonstrated in previous studies, this modified electrode can also be applied to study the electrocatalytic properties of biological molecules[44] and the reversible $NADH/NAD^+$ redox system.[45] The electrocatalytic activity for NADH oxidation is improved using the hybrid composites of PLM and nanomaterials.[46]

In the present investigation, luminol (LM), a versatile chemical and neutral red (NR), and a phenazine redox dye have been proposed to co-immobilize on an electrode surface because they have an amino group located on the heteroaromatic ring, which makes them amenable to facilitate electropolymerization,[44,47,48] and their good activities also have been gradually disclosed in the literature.[44,46,48,49] The use of GO and MWCNTs to improve the hybridization of conducting polymers and the electrocatalytic property is also studied.

In this work, a simple electrochemical synthesis of PLM and PNR hybrid films is studied using an active MWCNT–GO-electrode. The PLM–PNR–MWCN–GO hybrid nanocomposite can be easily prepared on an electrode surface through electropolymerization of LM and NR monomers using a suitable arrangement of MWCNTs and GO as an active and steric template. The hybrid composites are electrochemically characterized and the electrocatalytic oxidation of NADH is also investigated.

2. Experimental

2.1 Reagents and materials

Nicotinamide adenine dinucleotide (NADH), luminol (LM), neutral red (NR), and multi-walled carbon nanotubes (MWCNTs) were purchased from Sigma-Aldrich (USA) and were used as-received. All other chemicals (Merck) used were of analytical grade (99%). Double-distilled deionized water (>18.1 $M\Omega\ cm^{-1}$) was used to prepare all the solutions. All other reagents were of analytical grade and used without further purification. A pH 5.5 phosphate buffer solution (PBS) was prepared with 0.05 M Na_2HPO_4 and 0.05 M NaH_2PO_4 and adjusted to pH 5.5 with phosphoric acid.

2.2 Apparatus and measurements

The PLM–PNR–MWCNT–GO hybrid composite was characterized by cyclic voltammetry, UV-visible spectroscopy, SEM, AFM, and amperometry. A glassy carbon electrode (GCE) was purchased from Bioanalytical Systems (BAS) Inc., USA. All GCEs used had a diameter of 0.3 cm (exposed geometric surface area of $A = 0.0707\ cm^2$) for all electrochemical techniques. Electrochemical experiments were carried out using a CHI 1205a electrochemical workstation (CH Instruments, USA) with a conventional three-electrode setup containing a GCE, an Ag/AgCl (3 M KCl) electrode, and a platinum wire as working, reference, and counter electrodes, respectively. The buffer solution was entirely deaerated using a nitrogen gas atmosphere. The morphological characterization of composite films was examined by means of a SEM (S-3000H, Hitachi) and AFM images were recorded with a multimode scanning probe microscope (Being Nano-Instruments CSPM-4000, China). Indium tin oxide (ITO) substrates were used in morphological analysis for convenience.

2.3 Fabrication of PLM–PNR and PLM–PNR–MWCNT–GO modified electrodes

The electropolymerization of luminol (LM) and neutral red (NR) was carried out in pH 5.5 PBS containing 1.5×10^{-3} M LM and 1×10^{-4} M NR by consecutive cyclic voltammetry. Potential cycling was controlled in the potential range of −0.7 to +0.6 V with a scan rate of 0.1 V s^{-1} and 15 scan cycles. Both bare and MWCNT–GO modified electrodes were used for the electropolymerization of LM and NR.

The MWCNT–GO modified electrode was prepared by two steps: first, the electrochemical reduction of graphene oxide (GO), and then the adsorption of MWCNTs. The GO-modified electrode was prepared using the following procedures: first, the GO solution (0.5 mg ml^{-1}) was prepared in 0.5 M sulfuric acid, then, electrochemical reduction of GO was achieved by employing consecutive cyclic voltammetry in the potential range of 0 to −1.4 V (15 cycles, scan rate = 0.05 V s^{-1}). All MWCNTs were carboxylic functionalized and well-dispersed in PBS (1 mg ml^{-1}) with sonication for 10 minutes. By drop-casting, 10 μl of the solution was dropped onto the electrode surface and dried out in an oven at 40 °C. Consequently, the MWCNT–GO modified electrode was transferred to result in hybrid electropolymerization of LM and NR in pH 5.5 PBS containing 1.5×10^{-3} M LM and 1×10^{-4} M NR by consecutive cyclic voltammetry. After these procedures, the LM–PNR and PLM–PNR–MWCNT–GO modified electrodes were prepared for the study.

3. Results and discussion

3.1 Preparation and characterization of the PLM–PNR–MWCNT–GO hybrid composite

Hybridization of PLM and PNR is studied due to their activities and easy electropolymerization of monomers. However, the electropolymerization of two kinds of monomers might suffer from the difficulty of the disorder of polymer chains. Fig. 1A

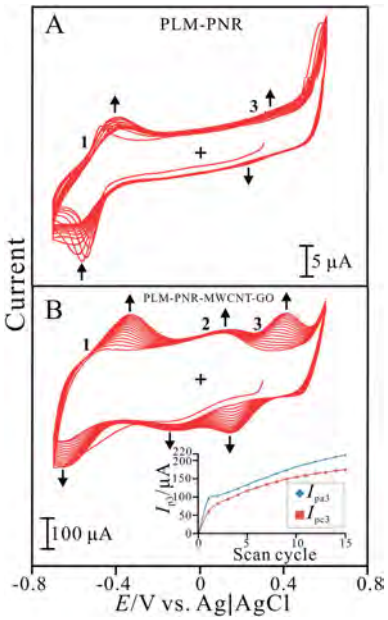

Fig. 1 Consecutive cyclic voltammograms of LM and NR electropolymerization using a (A) bare GCE and (B) MWCNT–GO/GCE examined in pH 5.5 PBS containing 1.5×10^{-3} M luminol and 1×10^{-4} M neutral red. Scan rate = 0.1 V s^{-1}.

shows the consecutive cyclic voltammograms of LM and NR electropolymerization using a bare GCE. Poor current development of redox peaks indicates that the hybrid electropolymerization of LM and NR is not perfect. In our strategy, MWCNT–GO was used as a conductive and steric substrate to enhance the hybrid electropolymerization of hetero-monomers (LM and NR) on the electrode surface. Fig. 1B shows the consecutive cyclic voltammogram of LM and NR electropolymerization using a MWCNT–GO/GCE. The cyclic voltammogram depicts significant current development of LM and NR electropolymerization at the MWCNT–GO/GCE better than that of the bare GCE. It exhibits three obvious redox couples with formal potentials of $E_1^{0\prime} = -0.5$ V, $E_2^{0\prime} = 0$ V, and $E_3^{0\prime} = +0.27$ V, related to NR, PNR (redox couples 1 and 2) and PLM (redox couple 3), respectively. Good current development is recorded in the plot of peak current *vs.* scan cycle (inset of Fig. 1B). Both anodic and cathodic peak currents increase with the increase of the scan cycles. It indicates that MWCNT–GO can effectively enhance the hybrid electropolymerization of hetero-monomers (LM and NR). Considering the previous report,[50] a novel hybrid nanomaterial (GO–MWNT) was explored based on the self-assembly of multi-walled carbon nanotubes (MWNTs) and graphene oxide (GO), which can cause positively charged horseradish peroxidase (HRP) to immobilize on GO–MWCNTs by the electrostatic interaction. So, this phenomenon indicates that the conductive and steric MWCNT–GO structure can provide more active sites to load the positively charged PLM and PNR, avoiding the disorder of polymer chains. One can conclude that the hybrid film formation of PLM and PNR can be improved by MWCNT–GO.

The experiment was designed to understand the spectra of these materials in the solution by UV-visible spectroscopy. Fig. S1† shows the UV-visible spectra of different materials and mixtures prepared in pH 7 PBS. The UV-visible spectrum of GO shows an absorption peak at 227 nm accompanied by a minor absorption peak at 300 nm. The spectrum of MWCNT shows an absorption peak at 253 nm. The spectrum of their mixture exhibits absorption peaks at 239 nm and 300 nm resulting from the overlapping of GO and MWCNT spectra. NR shows absorption peaks at 276 nm and 528 nm while LM shows absorption peaks at 218 nm, 300 nm, and 347 nm. The spectrum of their mixture exhibits absorption peaks (221 nm, 278 nm, 347 nm, and 531 nm) similar to their single spectrum. Furthermore, the spectrum of LM, NR, MWCNT, and the GO mixture also shows absorption peaks at 221 nm, 278 nm, 347 nm, and 531 nm similar to their single spectrum. These phenomena indicate that these materials can be mixed stably to form a stable hybrid composite.

Different material modified electrodes were prepared and studied by cyclic voltammetry. Fig. 2 shows the voltammograms of (a) PLM, (b) GO, (c) MWCNTs, (d) PNR, and (e) PLM–PNR–MWCNT–GO modified electrodes. PLM shows a redox couple with a formal potential of $E^{0\prime} = +0.27$ V while PNR shows two redox couples of $E^{0\prime} = -0.52$ V and $E^{0\prime} = +0.06$ V. No obvious redox couples can be found for GO and MWCNT. It means that no electrochemical process for these species. PLM–PNR–MWCNT–GO shows significant redox couples estimated with formal potentials of $E_1^{0\prime} = -0.51$ V, $E_2^{0\prime} = 0$ V, and $E_3^{0\prime} = +0.26$ V, related to NR, PNR (redox couples 1 and 2) and PLM (redox couple 3), respectively. It shows a high redox peak current which is several times higher than that of other modified electrodes. It indicates that the PLM–PNR–MWCNT–GO hybrid composite is

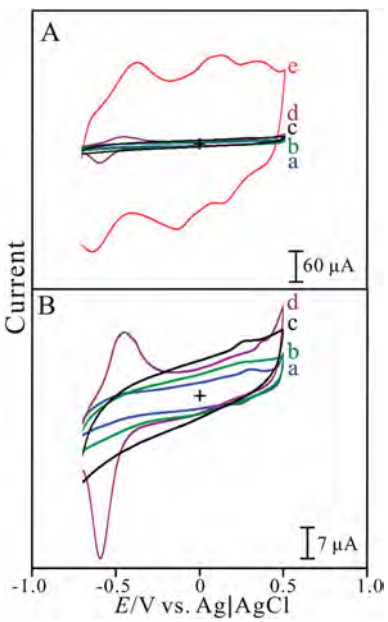

Fig. 2 (A) Cyclic voltammograms of different modifiers containing (a) PLM, (b) GO, (c) MWCNT, (d) PNR, and (e) PLM–PNR–MWCNT–GO modified GCEs examined in pH 7 PBS. (B) Scale-up voltammograms of (a) PLM, (b) GO, (c) MWCNT, and (d) PNR modified GCEs examined in pH 7 PBS. Scan rate = 0.1 V s^{-1}.

more reversible, active and compact among these modifiers. It also proves that the immobilization of PLM and PNR can be successfully enhanced by the highly conductive and steric MWCNT–GO structure.

The surface morphology of these modified electrodes was studied by SEM and AFM. Fig. S2† shows the SEM images of (A) GO, (B) MWCNT, (C) PLM, (D) PNR, (E) PLM–PNR, (F) MWCNT–GO, (G) PLM–PNR–GO, and (H) PLM–PNR–MWCNT–GO, respectively. Fig. S2A–D† exhibit single materials with unique structures of plane-like clusters (GO), steric clusters (MWCNT), snowflake clusters (PLM), and globular-like clusters (PNR), respectively. Fig. S2E† shows large clusters indicating that the hybridization of PLM and PNR is poor and not easy to generate nanocomposites without MWCNT–GO. Fig. S2F† displays the MWCNT–GO image before the hybridization of PLM and PNR polymers. It shows small clusters indicating that the electrochemical reduction of GO and the adsorption of MWCNTs to generate MWCNT–GO on the electrode surface are successful and compact. Fig. S2G and H† show the hybridization of PLM and PNR using GO and MWCNT–GO, respectively. By comparison, PLM–PNR–MWCNT–GO exhibits the structure of small fiber-like clusters. Considering the previous report,[50] this phenomenon can be explained by that MWCNT–GO can provide a more steric structure for the hybridization of PLM and PNR. They are further considered in AFM images.

Fig. 3 shows the AFM images of (A) PLM–PNR, (B) MWCNT–GO, (C) PLM–PNR–GO, and (D) PLM–PNR–MWCNT–GO, respectively. PLM–PNR shows less clusters without obvious images which might indicate that the hybridization is poor to generate hybrid films when compared to PLM–PNR–GO and PLM–PNR–MWCNT–GO images. When MWCNT–GO was immobilized on the electrode surface (Fig. 3B) it shows the plane-like and fiber-like structure. This phenomenon indicates that the conductive and high specific surface area can be constructed by our method. Particularly, PLM–PNR–MWCNT–GO shows specific porous mycelium-like nanostructures indicating that PLM and PNR nanofibers can be easily immobilized on MWCNT and GO due to their high conductivity and high specific surface area. The AFM images of these films show an average diameter of 67.5 nm, 13.7 nm, 11.6 nm, and 17.8 nm for PLM–PNR, MWCNT–GO, PLM–PNR–GO, and PLM–PNR–MWCNT–GO, respectively. These modifiers are proved in nanocomposites with an average roughness of 6.5 nm, 20.3 nm, 19.2 nm, and 22.6 nm, respectively. They display similar morphological properties in the results of SEM and AFM. One can conclude that the mycelium-like nanocomposite (PLM–PNR–MWCNT–GO) can be easily prepared by using a high conductive and high specific area (MWCNT–GO) to enhance the hybridization of different polymers (PLM and PNR).

The influence of the scan rate and pH condition on the PLM–PNR–MWCNT–GO/GCE electrochemical response was also studied. Fig. 4A shows the voltammograms of PLM–PNR–MWCNT–GO examined with a different scan rate of 10–500 mV s^{-1}. It shows three obvious redox couples with a small peak-to-peak separation and higher current response. Obvious redox couples indicate that PLM–PNR–MWCNT–GO can be well immobilized on the GCE and it shows a stable current response in the scan rate of 10–500 mV s^{-1}. PLM–PNR–MWCNT–GO has a small peak-to-peak separation indicating reversible and fast electron transfer processes. Both anodic and cathodic peak currents are directly proportional to the scan rate (inset of Fig. 4A), suggesting a surface controlled process in the electrochemical system. The observation of well-defined and persistent cyclic voltammetric peaks indicates that the PLM–PNR–MWCNT–GO/GCE exhibits electrochemical response

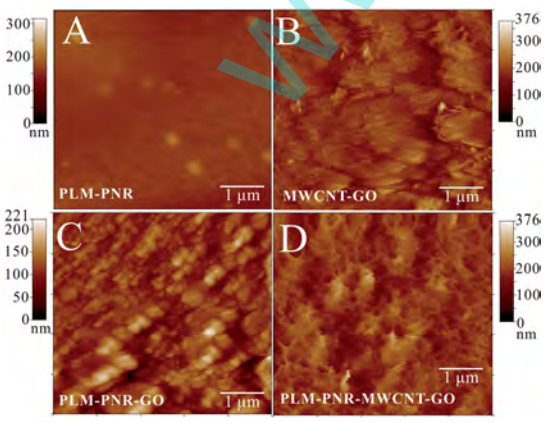

Fig. 3 AFM images of (A) PLM–PNR, (B) MWCNT–GO, (C) PLM–PNR–GO, and (D) PLM–PNR–MWCNT–GO coated ITO electrodes.

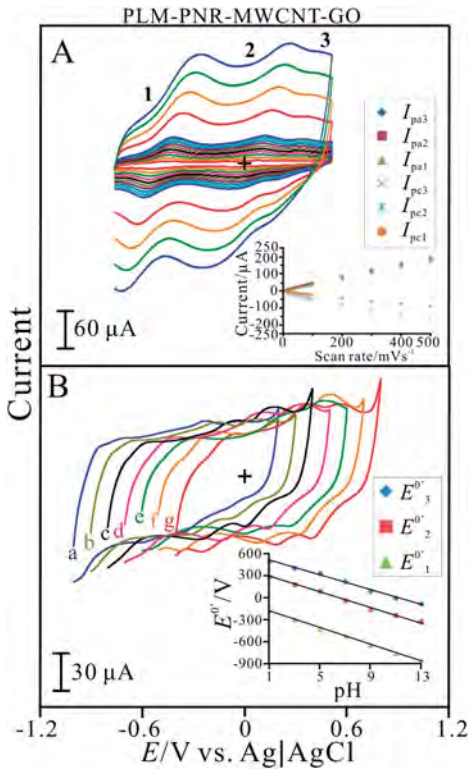

Fig. 4 Cyclic voltammograms of the PLM–PNR–MWCNT–GO/GCE examined with a (A) different scan rate: 10–500 mV s^{-1} (pH 7 PBS) and (B) different pH: 1–13 (scan rate = 0.1 V s^{-1}), respectively. Insets: the plots of peak current *vs.* scan rate and formal potential ($E^{0\prime}$) *vs.* pH.

characteristics of the redox species confined on the electrode. The apparent surface coverage (Γ) was estimated by the following equation:

$$I_p = n^2F^2vA\Gamma/4RT \quad (1)$$

where I_p is the peak current of the PLM–PNR–MWCNT–GO composite electrode; n is the number of electrons transfer; F is the Faraday constant (96 485 C mol^{-1}); v is the scan rate (mV s^{-1}); A is the area of the electrode surface (0.07 cm^2); R is the gas constant (8.314 J mol^{-1} K^{-1}); and T is the room temperature (298.15 K). Assuming a one-electron process for PLM and a two-electron process for NR and PNR in the present case, the Γ was calculated to be 4.04 × 10^{-9} mol cm^{-2}, 1.43 × 10^{-9} mol cm^{-2}, and 1.36 × 10^{-9} mol cm^{-2} for PLM, NR, and PNR, respectively.

The current response values are several times larger than those found in previous studies of PLM, NR, and PNR.[44,46,48,49] High surface coverage indicates that the hybrid composite might be compact with more electroactive species on the electrode surface. One can conclude that MWCNT–GO provides more active sites to load more electroactive species.

To ascertain the effect of pH, the PLM–PNR–MWCNT–GO/GCE was examined in different pH solutions (pH 1–13). Fig. 4B presents the PLM–PNR–MWCNT–GO redox peaks which are shifted to a more negative potential with the increasing pH value of the solution. It shows stable redox peaks under various pH conditions. This result is the same even though PLM–PNR–MWCNT–GO is repeatedly examined changing the testing order of the pH condition. It indicates that the PLM–PNR–MWCNT–GO hybrid composite is active and stable underwide pH conditions. The characteristic PNR redox couples (with formal potentials of $E_1^{0\prime}$ and $E_2^{0\prime}$) exhibit significant slopes of −56.7 mV pH^{-1} ($y = -56.7x - 127.4$, $R^2 = 0.997$) and −51.8 mV pH^{-1} ($y = -51.8x + 332.9$, $R^2 = 0.995$) for redox couples 1 and 2, respectively. The PLM redox couple ($E_3^{0\prime}$) is also pH-dependent with a slope of −50.3 mV pH^{-1} ($y = -50.3x + 564$, $R^2 = 0.995$). These slopes are close to that given by the Nernstian equation, suggesting a two-electron and two-proton transfer for NR and PNR redox processes.[48,49] For the PLM redox process, it is suggested as a one-electron and one-proton transfer compared with previous results.[44,46] It represents the electrochemical behavior through the reduction and oxidation states of PLM, NR and PNR and the results are also close to previous reports.[44,46,48,49] As a result, the hybrid composites can be stable and electroactive in different pH buffer solutions.

3.2 Electrocatalysis of NADH and the amperometric response at the PLM–PNR–MWCNT–GO electrode

The electrocatalytic activity of the PLM–PNR–MWCNT–GO electrode towards the oxidation of NADH in pH 7 PBS was investigated using cyclic voltammetry. Fig. 5 displays the voltammograms of the PLM–PNR–MWCNT–GO/GCE in pH 7 PBS with/without 5 × 10^{-4} M NADH. The PLM–PNR–MWCNT–GO/GCE shows two obvious oxidation peaks at about +0.1 V and +0.33 V for NADH. These two characteristic oxidation peaks are related to PNR and PLM redox processes indicating that PLM and PNR are active towards NADH oxidation.

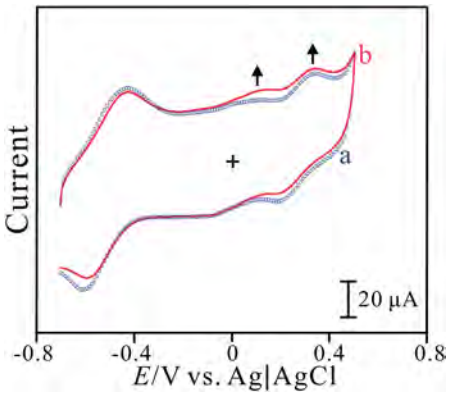

Fig. 5 Cyclic voltammograms of the PLM–PNR–MWCNT–GO/GCE examined in pH 7 PBS in the (a) absence and (b) presence of 5 × 10^{-4} M NADH.

In order to clarify the activity of the proposed PLM–PNR–MWCNT–GO hybrid composite, different modifiers were used for electrocatalytic oxidation of NADH. Fig. S3† shows the voltammograms of (a) GCE, (b) PLM–MWCNT–GO, (c) PLM–PNR–MWCNT, (d) PLM–PNR–GO, and (e) PLM–PNR–MWCNT–GO examined in pH 7 PBS containing 1 × 10^{-4} M NADH. The proposed composite shows a much higher current response in the presence of NADH compared to other modifiers. The activities of various modifiers are further evaluated by the anodic peak potential (E_{pa}) and net current response (ΔI_{pa}) as shown in Table S1.† By comparison, the anodic peaks for NADH oxidation are frequently found at about +0.15 V and +0.35 V, corresponding to our previous PLM–MWCNT system.[46] Moreover, these anodic peaks seem varying as different hybrid composites. One can see that the PLM–PNR–MWCNT–GO can provide comparable anodic peaks at +0.144 V and +0.369 V (with low overpotential compared to a bare GCE) and significant current responses ($\Delta I_{pa2} = 18.5$ μA and $\Delta I_{pa3} = 5.9$ μA) for NADH oxidation. One can conclude that the PLM–PNR–MWCNT–GO is electroactive and so it can be used as a good bioelectrocatalyst for NADH sensing.

Fig. 6A shows amperometric responses of a PLM–PNR–MWCNT–GO modified electrode with several additions of NADH obtained by amperometry. They were carried out with an electrode rotation speed of 5000 rpm and individually applied potential at +0.1 V. The PLM–PNR–MWCNT–GO/GCE shows significant amperometric responses for NADH additions spiked by micro-syringe. Inset (a) of Fig. 6A shows a low detection limit of 1.33 × 10^{-8} M ($S/N = 3$) and a short response time less than 10 s. Inset (b) of Fig. 6A presents the calibration curve, it provides two linear concentration ranges of 1.33 × 10^{-8} to 1.95 × 10^{-4} M and 2.08 × 10^{-4} to 5.81 × 10^{-4} M. The sensitivity is estimated to be 288.9 μA mM^{-1} cm^{-2} and 151.3 μA mM^{-1} cm^{-2} with the regression equations of I_{NADH} (μA) = 20.4C_{NADH} (μM) + 0.1 ($R^2 = 0.996$) and I_{NADH} (μA) = 10.7C_{NADH} (μM) + 1.9 (R^2 = 0.995), respectively. Two linear concentration ranges might be caused by the modifier's nature. In our viewpoints, the PLM–

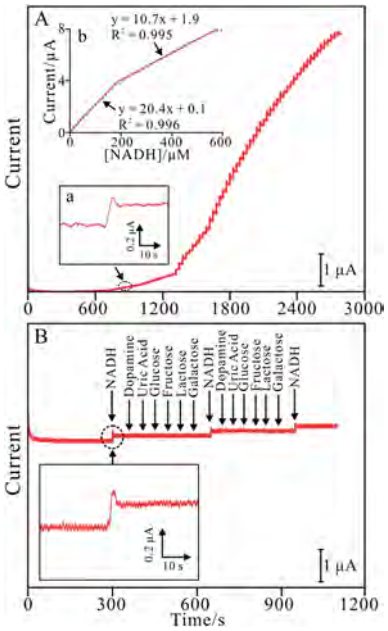

Fig. 6 Amperograms of the PLM–PNR–MWCNT–GO/GCE examined in pH 7 PBS containing (A) [NADH] = 1.33×10^{-8} to 5.94×10^{-4} M and (B) potential interferents: dopamine, uric acid, glucose, fructose, lactose, and galactose (1.33×10^{-5} M for each addition). Insets are the scale-up amperomogram and the calibration curve.

PNR–MWCNT–GO has some kind of concentration tolerance for NADH with specific linearity in the low (1.33×10^{-8} to 1.95×10^{-4} M) and high (2.08×10^{-4} to 5.81×10^{-4} M) concentration ranges. Having the above information, it would be easier to compensate the electronic signal of an NADH sensor for practical fabrication.

Table 1 presents the main performances of published data about NADH sensors based on different modified materials. They show competitive performance in the literature. By comparison, the NADH sensor presented in this paper exhibits one of the highest sensitivity with a low detection limit and low overpotential. A significant lower detection limit and higher sensitivity were reported for sensors based on MWCNTs. It might be caused by the synergistic effect of the obtained CNT/conducting polymer which has the properties of the individual components similar to those shown in previous reports.[18–23]

One can conclude that the active hybrid composite shows competitive performance towards other materials (Table 1). It has the excellent ability to determine NADH due to the low detection limit, low working potential, and high current response, suggesting that it is a highly sensitive NADH sensor.

3.3 Interference study of the PLM–PNR–MWCNT–GO composite

The PLM–PNR–MWCNT–GO modified electrode was studied with the interference effect on the amperometric response for NADH. It was examined in the presence of several interferents including ascorbic acid, dopamine, uric acid, glucose, fructose, lactose, and galactose ($E_{app.}$ = +0.1 V). Fig. 6B shows the amperometric response of PLM–PNR–MWCNT–GO with various interferents. No interference occurred in the amperograms except for the case of ascorbic acid. It was further applied to study the correlation between the current response and potential compared to a bare electrode by linear sweep voltammetry (LSV). Fig. S4A† shows the LSV voltammograms of PLM–PNR–MWCNT–GO examined in the presence of ascorbic acid and NADH. It shows similar oxidation peaks for ascorbic acid and NADH so that it is further considered using a bare electrode. Fig. S4B† shows the LSV voltammograms of a bare electrode examined in the presence of ascorbic acid, NADH, and their mixture. The inset of Fig. S4B† presents the relationship between the peak current and species. A good correlation is found at +0.45 V, and it is noticed that the current response of the AA + NADH mixture is almost twice that of AA. This information indicates that NADH can be determined more exactly by inspection of ascorbic acid using a bare electrode. This phenomenon might be explained by the overpotential of AA and NADH. In our viewpoint, a bare GCE can show different anodic peaks at +0.2 V and +0.45 V, corresponding to their overpotentials for AA and NADH, respectively. Here we have two conclusions: (i) one might gain the accumulated current response in the voltammograms after scanning across the overpotential of all electroactive analytes; and (ii) the

Table 1 Performance for sensing NADH with various material modified electrodes

Modified materials	$E_{app.}$[a] (V) *vs.* Ag/AgCl	LOD[b] (μM)	Sensitivity (μA mM^{-1} cm^{-2})	Ref.
Polyluminol/MWCNT	0.10	0.6	183.9	46
PNR–FAD	0.10	10	21.5	49
Highly ordered mesoporous carbon	0.25	1.61	93	51
Chemically reduced graphene oxide	0.45	10	2.68	52
Graphite/PMMA	0.45	3.5	68	53
MWCNT/poly-Xa	0.45	0.1	2.2	54
ERGO–PTH/GC	0.40	0.1	143	55
Poly-Xa/FAD/MWCNT	0.15	171	155	56
PAH/SPE	0.60	0.22	125.9	57
PLM–PNR–MWCNT–GO	0.10	0.0133	288.9	This work

[a] $E_{app.}$ = applied potential. [b] LOD = limit of detection.

accumulated current responses at +0.2 V and +0.45 V might provide information about the NADH/AA ratio in the mixture. One can conclude that the modified electrode can avoid interference from most of the interferents, being a good electrocatalyst for determination of NADH.

3.4 Stability study of the PLM–PNR–MWCNT–GO modified electrodes

The reproducibility and stability of the sensor were evaluated. Five PLM–PNR–MWCNT–GO electrodes were investigated at +0.1 V to compare their amperometric current responses. Ten successive measurements of NADH on one PLM–PNR–MWCNT–GO electrode yielded an R.S.D. of 2.1%, indicating that the sensor was stable and highly reproducible. The long-term stability of the sensor was also evaluated by measuring its current response to NADH within a 7 day period. The sensor was stored at 4 °C and its sensitivity was tested every day. The current response of the PLM–PNR–MWCNT–GO electrode was approximately 93% of its original counterpart, which can be mainly attributed to the chemical stability of PLM and PNR on MWCNT–GO.

4. Conclusions

PLM and PNR hybrid films can be successfully prepared on an electrode surface and further enhanced by MWCNT–GO. PLM–PNR–MWCNT–GO shows a specific mycelium-like nanostructure indicating that PLM and PNR nanofibers can be easily immobilized on MWCNTs and GO due to their high conductivity and high specific surface area. The modified electrode is electrochemically characterized and examined as a novel NADH sensor, which presents attractive analytical features such as high sensitivity, low overpotential, low detection limits, good stability, and good reproducibility.

Acknowledgements

We acknowledge the National Science Council (project no. NSC1012113M027001MY3), Taiwan.

Notes and references

1 L. Gorton and E. Dominguez, Electrochemistry of NAD(P)$^+$/NAD(P)H in *Encyclopedia of Electrochemistry*, Wiley-VCH, Weinheim, 2002, vol. 9, pp. 67–143.
2 S. Liu, Z. Du, P. Li and F. Li, *Biosens. Bioelectron.*, 2012, **35**, 443–446.
3 Y. P. Hung, J. G. Albeck, M. Tantama and G. Yellen, *Cell Metab.*, 2011, **14**, 545–554.
4 W. D. Koning and K. V. Dam, *Anal. Biochem.*, 1992, **204**, 118–123.
5 K. Yamada, N. Hara and T. Shibata, *Anal. Biochem.*, 2006, **352**, 282–285.
6 F. Sadanaga-Akiyoshi, H. Yao and S. Tanuma, *Neurochem. Res.*, 2003, **28**, 1227–1234.
7 W. J. Xie, A. S. Xu and E. S. Yeung, *Anal. Chem.*, 2009, **81**, 1280–1284.
8 H. Yao, H. B. Halsall, W. R. Heineman and S. H. Jenkins, *Clin. Chem.*, 1995, **41**, 591–598.
9 X. He, X. Ni, Y. Wang, K. Wang and L. Jian, *Talanta*, 2011, **83**, 937–942.
10 A. Bergel, J. Souppe and M. Comtat, *Anal. Biochem.*, 1989, **179**, 382–388.
11 Y. Yan, W. Zheng, L. Su and L. Mao, *Adv. Mater.*, 2006, **18**, 2639–2643.
12 A. Radoi and D. Compagnone, *Bioelectrochemistry*, 2009, **76**, 126–134.
13 J. Moiroux and P. J. Elving, *Anal. Chem.*, 1978, **50**, 1056–1062.
14 Z. Samec and P. J. Elving, *J. Electroanal. Chem.*, 1983, **144**, 217–234.
15 W. J. Blaedel and R. A. Jenkins, *Anal. Chem.*, 1975, **47**, 1337–1343.
16 M. Musameh, J. Wang, A. Merkoci and Y. Lin, *Electrochem. Commun.*, 2002, **4**, 743–746.
17 M. G. Zhang, A. Smith and W. Corski, *Anal. Chem.*, 2004, **76**, 5045–5050.
18 C. Deng, J. Chen, X. Chen, C. Xiao, Z. Nie and S. Yao, *Electrochem. Commun.*, 2008, **10**, 907–909.
19 R. H. Baughman, A. A. Zakhidov and W. A. D. Heer, *Science*, 2002, **297**, 787–792.
20 P. R. Lima, W. D. J. R. Santos, A. B. Oliveira, M. O. F. Goulart and L. T. Kubota, *Biosens. Bioelectron.*, 2008, **24**, 448–454.
21 S. Hrapovic, Y. Liu, K. B. Male and J. H. T. Luong, *Anal. Chem.*, 2004, **76**, 1083–1088.
22 J. Sandler, M. Schaffer, T. Prasse, W. Bauhofer, K. Schulte and A. H. Windle, *Polymer*, 1999, **40**, 5967–5971.
23 C. Y. Wei, D. Srivastava and K. J. Cho, *Nano Lett.*, 2002, **2**, 647–650.
24 M. G. Hughes, Z. Chen, M. S. P. Schaffer, D. J. Fray and A. H. Windle, *Chem. Mater.*, 2002, **14**, 1610–1613.
25 K. H. An, S. Y. Jeong, H. R. Hwang and Y. H. Lee, *Adv. Mater.*, 2004, **16**, 1005–1009.
26 E. Kymakis and G. A. J. Amaratunga, *Appl. Phys. Lett.*, 2002, **80**, 112–114.
27 H. S. Woo, R. Czerw, S. Webster, D. L. Carroll, J. W. Park and J. H. Lee, *Synth. Met.*, 2001, **116**, 369–372.
28 I. Musa, M. Baxendale, G. A. J. Amaratunga and W. Eccleston, *Synth. Met.*, 1999, **102**, 1250–1254.
29 J. N. Coleman, S. Curran, A. B. Dalton, A. P. Davey, B. McCarthy, W. Blau and R. C. Barklie, *Synth. Met.*, 1999, **102**, 1174–1175.
30 A. K. Geim and K. S. Novoselov, *Nat. Mater.*, 2007, **6**, 183–191.
31 J. M. Parpia, H. G. Craighead and P. L. McEuen, *Science*, 2007, **315**, 490–493.
32 S. Gilje, S. Han, M. Wang, K. L. Wang and R. B. Kaner, *Nano Lett.*, 2007, **7**, 3394–3398.
33 F. Schedin, A. K. Geim, S. V. Morozov, E. W. Hill, P. Blake, M. I. Katsnelson and K. S. Novoselov, *Nat. Mater.*, 2007, **6**, 652–655.
34 V. C. Tung, J. H. Huang, I. Tevis, F. Kim, J. Kim, C. W. Chu, S. I. Stupp and J. X. Huang, *J. Am. Chem. Soc.*, 2011, **133**, 4940–4947.

35 J. H. Huang, J. H. Fang, C. C. Liu and C. W. Chu, *ACS Nano*, 2010, **5**, 6262–6271.
36 C. Deng, F. Qu, H. Lu and M. Yang, *Biosens. Bioelectron.*, 2011, **26**, 4810–4814.
37 S. Ge, M. Yan, J. Lu, M. Zhang, F. Yu, J. Yu, X. Song and S. Yu, *Biosens. Bioelectron.*, 2012, **31**, 49–54.
38 T. Y. Huang, J. H. Huang, H. Y. Wei, K. C. Ho and C. W. Chu, *Biosens. Bioelectron.*, 2013, **43**, 173–179.
39 S. He, W. Shi, X. Zhang, J. Li and Y. Huang, *Talanta*, 2010, **82**, 377–383.
40 J. Rong, Y. Chi, Y. Zhang, L. Chen and G. Chen, *Electrochem. Commun.*, 2010, **12**, 270–273.
41 X. M. Chen, B. Y. Su, X. H. Song, Q. A. Chen, X. Chen and X. R. Wang, *Trends Anal. Chem.*, 2011, **30**, 665–676.
42 X. Yang, Y. Guo and A. Wang, *Anal. Chim. Acta*, 2010, **666**, 91–96.
43 D. Tian, C. Duan, W. Wang and H. Cui, *Biosens. Bioelectron.*, 2010, **25**, 2290–2295.
44 S. M. Chen and K. C. Lin, *J. Electroanal. Chem.*, 2002, **523**, 93–105.
45 K. C. Lin and S. M. Chen, *J. Electroanal. Chem.*, 2006, **589**, 52–59.
46 K. C. Lin, C. Y. Yin and S. M. Chen, *Analyst*, 2012, **137**, 1378–1383.
47 A. A. Karyakin, E. E. Karyakina and H. L. Schmidt, *Electroanalysis*, 1999, **11**, 149–155.
48 S. M. Chen and K. C. Lin, *J. Electroanal. Chem.*, 2001, **511**, 101–114.
49 K. C. Lin, Y. C. Lin and S. M. Chen, *Analyst*, 2012, **137**, 186–194.
50 Q. Zhang, S. Yang, J. Zhang, L. Zhang, P. Kang, J. Li, J. Xu, H. Zhou and X. M. Song, *Nanotechnology*, 2011, **22**, 494010.
51 M. Zhou, L. Shang, B. Li, L. Huang and S. Dong, *Electrochem. Commun.*, 2008, **10**, 859–863.
52 M. Zhou, Y. Zhai and S. Dong, *Anal. Chem.*, 2009, **81**, 5603–5613.
53 H. Dai, H. Xu, Y. Lin, X. Wu and G. Chen, *Electrochem. Commun.*, 2009, **11**, 343–346.
54 F. D. A. D. S. Silva, C. B. Lopes, E. D. O. Costa, P. R. Lima, L. T. Kubota and M. O. F. Goulart, *Electrochem. Commun.*, 2010, **12**, 450–454.
55 Z. Li, Y. Huang, L. Chen, X. Qin, Z. Huang, Y. Zhou, Y. Meng, J. Li, S. Huang, Y. Liu, W. Wang, Q. Xie and S. Yao, *Sens. Actuators, B*, 2013, **181**, 280–287.
56 K. C. Lin, Y. S. Li and S. M. Chen, *Sens. Actuators, B*, 2013, **184**, 212–219.
57 L. Rotariu, O. M. Istrate and C. Bala, *Sens. Actuators, B*, 2014, **191**, 491–497.